Aero Structural Modeling of a Wing Using CATIA V5 And XFLR5 Software And Experimental Validation Using The Price-Païdoussis Wing Tunnel

Conference Paper · June 2015

DOI: 10.2514/6.2015-2558

CITATIONS
16

READS
11,665

4 authors:

David Communier
École de Technologie Supérieure
7 PUBLICATIONS **58** CITATIONS
SEE PROFILE

Manuel Flores Salinas
École de Technologie Supérieure
10 PUBLICATIONS **75** CITATIONS
SEE PROFILE

Oscar Carranza
École de Technologie Supérieure
4 PUBLICATIONS **21** CITATIONS
SEE PROFILE

Ruxandra Mihaela Botez
École de Technologie Supérieure
541 PUBLICATIONS **4,882** CITATIONS
SEE PROFILE

Aero Structural Modeling of a Wing Using CATIA V5 And XFLR5 Software And Experimental Validation Using The Price-Païdoussis Wing Tunnel

David Communier.[1], Manuel Flores Salinas[2], Oscar Carranza Moyao[3]
and Ruxandra Mihaela Botez[4]
ETS, LARCASE, 1100 Notre Dame West, Montreal, Qc, Canada

During the structural study of an aircraft wing, it is difficult to accurately model the aerodynamic forces applied on the wing. To facilitate analysis, the lift of the wing is distributed on the main wing's spar and its ribs. This method particularly works when the wing structure has a main beam. At this point; we design this spar so that it can withstand the lift of the wing on its own. This implies that the entire wing will be stronger than necessary so that the structure will not be fully optimized. To overcome this problem, we should be able to apply an overall aerodynamic distribution over the entire surface of the wing. By applying realistic embedment, we should be able to get much more reliable results. To achieve this we will therefore need to combine the software results of calculations about the aerodynamics of a wing with the software results for its design and structural analysis. In this project, the software used to calculate the coefficients of pressure on the wing is XFLR5 and the software for the design and structural analysis will be CATIA V5.The XFLR5 software allows quick analysis of a wing based on the analysis of its airfoils. This software computes airfoil performances as XFoil and lets you choose from three methods to calculate the performance of the wing (LLT, VLM and 3D Panels). To validate the results given by XFLR5, wind tunnel tests were performed on several different airfoils. Regarding the design and finite-element analysis of the structure, the CATIA V5 software is commonly used in the aerospace field. It is easier and faster to use than software like HyperMesh and gives very similar results. CATIA V5 also provides greater automation steps for wing design. Thus, in this project we will see how to automate the design process from the reading of the results obtained by XFLR5, specifically about the pressures around the wing, to the creation of the skin representing the surface of the wing. The goal to achieve, after a quick analysis on XFLR5 and a recording of values of the pressure coefficient, the user would only have to launch a CATIA V5 program to get the skin of the wing with the applied pressures. Once the skin is obtained, the user can create the inside structure of the wing and during the structural analysis, the deformation of the wing can realistically be visualized and thus optimized for the best possible structure.

Nomenclature

SYMBOLES

α	angle of incidence
ρ	air density
I_G	inertia about the center of gravity
S	wing surface
v	velocity
Axis	
X	horizontal axis of a sketch
Y	vertical axis of a sketch
Coefficient	
C_L, C_D, C_M	lift, drag and pitch coefficients
CP	coefficient of pressure

[1] Insert Job Title, Department Name, Address/Mail Stop, and AIAA Member Grade for first author.
[2] Insert Job Title, Department Name, Address/Mail Stop, and AIAA Member Grade for second author.
[3] Insert Job Title, Department Name, Address/Mail Stop, and AIAA Member Grade for third author.
[4] Insert Job Title, Department Name, Address/Mail Stop, and AIAA Member Grade for fourth author (etc).

Contraint

σ	applied stress
σ_M	maximum material strain

Thread

¼-20	impérial 0.25po diameter
M3	métrique 3mm diameter
M8	métrique 8mm diameter

Force and moment

D	drag
F	applied force
L	lift
M	pitch

Lenght

b	wing span
C	wing cord
h	thickness of the spar
t_u	thickness of the upper spar

Subscript

i	loop index increment
tip	wingtip cord
root	root cord

Wing axis

X	longitudinal
Y	side
Z	vertical

I. Introduction

In order to optimize the structure of a wing, a good pressure distribution around the wing is required. When optimizing the structure, the applied forces values are simplified to calculate its deformations. These simplifications involved a margin of error and therefore a less optimized structure than the desired one was obtained. A new technique using the distribution of the pressure coefficients around the wing is presented in this paper. This technique combines aerodynamic analysis [1] performed using the XFLR5 software with structural analysis using CATIA V5 [2].

The proposed methodology is divided into two principal parts that are explained in sections 2 and 4. In the first section of the paper, an aerodynamic analysis of a wing using XFLR5 is performed, and in the third section, a structural wing analysis is performed using finite elements calculation in CATIA V5.

In section 3, the validation of aerodynamic calculation using XFLR5 is performed. The use of this calculation tool being new in our laboratory, we have performed tests in the Price-Païdoussis subsonic wind tunnel at the LARCASE, ETS in order to compare, and thus to validate the theoretical aerodynamic theoretical values with experimental values. The particularity of this methodology is that pressure coefficients computed with XFLR5 are applied on the wing surface modeled by finite elements methodologies in CATIA V5.

II. Numerical Calculation Of Pressure Coefficients Using XFLR5 Code

The distribution of the pressure coefficients on the wing surface are calculated with the aim to obtain the wing aerodynamic performances. Two software can be used, the ANSYS – Fluent calculator [4], or the XFLR5 (Lifting Line Theory LLT, Vortex Lattice Method VLM, 3D Panels). Because of the fact that the XFRL5 software is optimized for wing performances calculations, it is preferred to ANSYS – Fluent to be used for our methodology. The XFLR5 - LLT and - VLM methods do not provide the pressure distribution on the wing surface, and for this reason, the 3D Panels method was used to obtain the pressures distribution values. A grid is created using the 3D Panels on the wing surface to be studied. This created grid allows the assignation of a pressure coefficient on each grid cell. The coefficients being dimensionless, final wing dimensions are adjusted without having to redo all the aerodynamic pressure calculations. In the case of a wing analysis, the structural study could be done at the same time as the aerodynamic study. Indeed, if the aerodynamic study indicates that it would be important to modify the wing chord, its span or any other geometric parameters, then the structural model parameterisation would allow these modifications to be done without having to do over again the modelisation.

A. Application of the 3D Panels method

The 3D Panels method consists of meshing the wing surface with panels, and performing aerodynamic calculations on each created panels. It means that meshing the surface in order to make a finite-element model but with the particularity that using this method, results can be obtained with fewer meshes, that means with smaller computer execution time. To perform the analysis of a wing, we need to import the airfoils coordinates used for its design. In order to import the airfoils from a text file, the file must respect a specific format, which means, that the first line must contain the name of the airfoil (optional choice), followed by the X and Y coordinates of the airfoil starting their numerotation from the trailing edge. XFLR5 code uses a C++ translation of the XFoil software code (initially in FORTRAN) to generate performance aerodynamic results which are starting points for airfoil analysis. The calculations used are identical to the XFoil software calculation, but XFLR5 code mainly offers a more evolved and intuitive user interface compared to XFoil code, along with additional functionalities such as wing analysis and stability analysis. Figure 1 shows the type of results that could be obtained. Namely, wing performance curves such as lift coefficient with the angle of attack, drag coefficient with the angle of attack, thickness of the wing with angle of attack, etc. In this example, the S1223 airfoil was used. The 'S' in the name of the airfoil indicates that it has been drawn by Doctor Michael S. Selig. The curves displayed are customizable, so it is possible to show only the needed information.

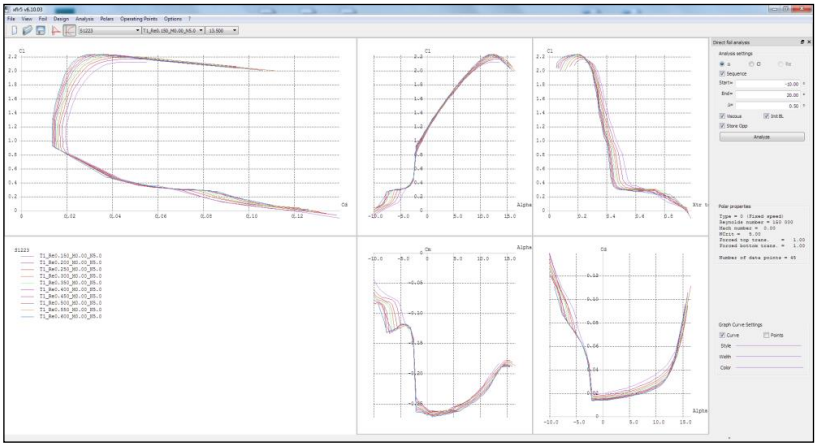

Figure 1. Display of performance curves for the S1223 airfoil in XFLR5 code.

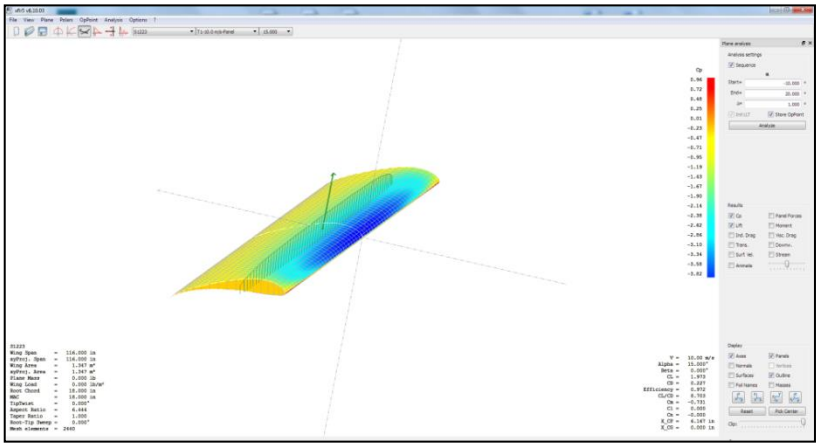

Figure 2. Display of pressure coefficients on XFLR5.

The 3D Panels calculation method computes the aircraft performances based on its geometries [5]. Thus, the lift and drag of the wing are obtained. However, this method by itself does not provide the induced drag. In order to obtain the induced drag, it is necessary to perform additional calculations in XFLR5 code based on the performances of the airfoil at different Reynolds numbers. From that analysis, the performance characteristics of the wing can be obtained. Those performances can be

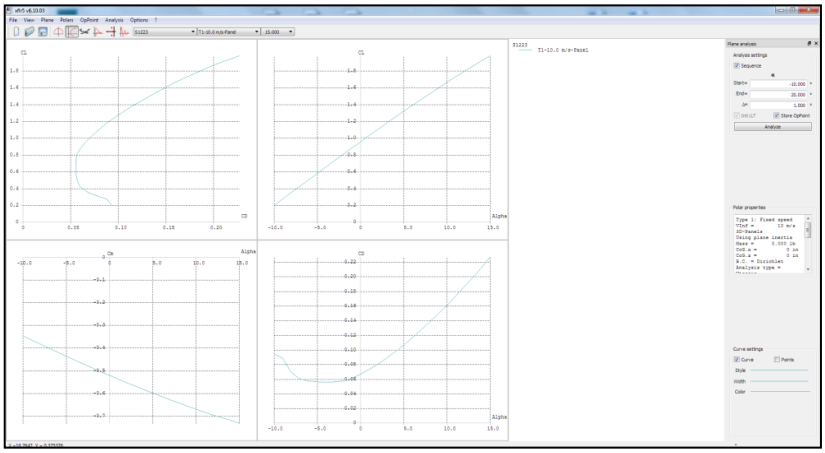

Figure 3. Performance curves of a S1223 airfoil wing using XFLR5 code.

visualized by different means. A relevant display for our methodology is to view the wing with the pressure coefficients around it, as shown in figure 2. Another way is to display the performance curves of the wing similarly as the ones obtained for the airfoil. Those curves are shown in figure 3. Same logic applies to the display of the airfoil curves, where the parameters to be viewed could be selected according to is the needed result, such as variation of lift and drag coefficients with angle of attack.

B. Comparison between the results obtained in XFLR5 and those obtained by wind tunnel tests

By using the XFLR5 software to compute wing performances, we can choose from various methods (LLT, VLM or 3D Panels). In order to choose the best method from the three ones, there is an additional extrapolation calculation based on the analysis of the wing airfoil to obtain the induced drag. Following this choice, tests were conducted in the Price-Païdoussis subsonic wind tunnel at the LARCASE, ETS to verify the accuracy of this analysis with the aim to validate experimentally the numerical values obtained. The objective is to obtain an accurate analysis of the aero-structural interactions, where the accuracy of the calculations was very important. In order to compare the obtained results, the variations of the lift, drag and pitching moment coefficients as functions of the angle of attack were first numerically traced. The XFLR5 – 3D Panels methodology provided these values for the studied wing (figure 3).

C. Export of pressure coefficients from XFLR5

Using the XFLR5 software, the pressure coefficients around the surface of the wing can be exported as a text file (figure 4). The pressure coefficients can be imported using a text file into the wing model in CATIA V5. In XFLR5, the wing surface is meshed into rectangles, and mean values of pressure coefficients applied to each of those rectangles are computed. Thus, the wing surface can then be recreated from the coordinates of those same pressure coefficients. The wing is generated from a single file containing the coordinates of the pressure coefficients. Thus, errors related to the application of the pressures on the surface of the wing are avoided. Then the XFLR5 grid obtained in figure 2 must be recreated on the wing surface generated in CATIA V5. The grid in CATIA V5 depends on the number of airfoils coordinates and thus, the use of multiple files might cause errors if the number of points in the coordinates file imported on CATIA V5 does not match the grid exported from XFLR5. No errors in this type of work were found.

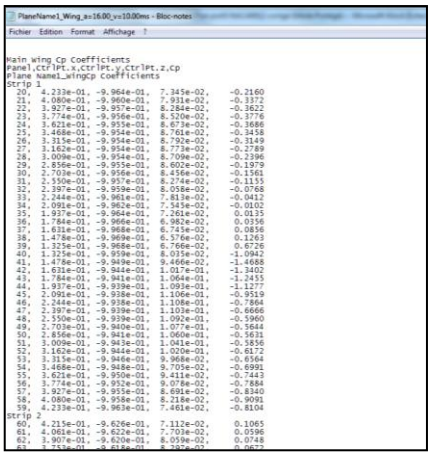

Figure 4. Text File containing the pressure coefficients coordinates.

III. Validation Of Numerical Results Using The Price-Païdoussis Subsonic Wind Tunnel

A. Aerodynamic balance

In order to obtain the lift, drag and moment wing's experimental coefficients variation with the angle of attack, an aerodynamic balance has been designed and built in house. This balance consisted of two aluminum plates attached to a force sensor, where one of the plates was fixed to the base of the test chamber, in the wind tunnel. The force sensor used was the Mini45-E from the Array Technology Incorporated (ATI) company, and is represented in figure 5. In order to change the angle of attack of the wing while keeping the wing fixed during each test of a flight condition, an efficient system of rotating plates was designed, and further used for performing all tests in the Price-Païdoussis subsonic wind tunnel. This system provides an accuracy of the relative displacement of the angle of attack of 0.5 degrees. On the current system, the angle shifting is done manually but it could be automated. After the setting up of the system, we were able to obtain the lift, drag forces and the moment variation with the angle of attack. During the tests, the speed was

Figure 5. ATI sensor fixed on the aluminum plate.

controlled, and the air density was measured. Since the dimensions of the chosen wing surface are known during the tests, the aerodynamic coefficients of the wing were experimentally obtained and further compared to the calculated theoretical values generated by XFLR5 code.

B. Subsonic Price-Païdoussis Wind Tunnel

The LARCASE – Price-Païdoussis open blow down subsonic wind tunnel has a length of 12 m is used to test and validate Computational Fluid Dynamics (CFD) models [6]. At the LARCASE, research on morphing wing testing and validation on the IAR-NRC wind tunnel has been performed [7] - [17]. This wind tunnel gives an efficient control over the flow conditions, as well as accurate measurements of the pressures distribution on a wing. In the beginning of tests, the air pressure rises through the centrifugal fan by creating a lateral mixture of the fluid layers. The agitated particles are redirected by the filters, and a laminar flow is obtained. The wind tunnel shown in figure 6 consists of a centrifugal fan, a diffuser and settling chamber, a contraction section and a working section. The dimensions of the different sections are indicated in figure 7. The centrifugal fan is powered by a North Western Electric Co. electrical engine of 40 Hp and 67 A. This DC motor has a Silicon-Controlled-Redressor (SCR) and thus, it can be powered by any conventional 120 VAC outlet.

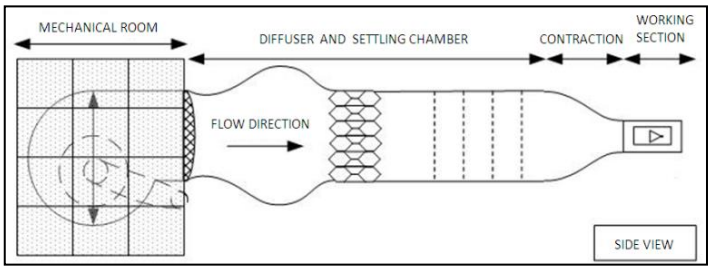

Figure 6. Sections of the Price-Païdoussis subsonic blow down wind tunnel.

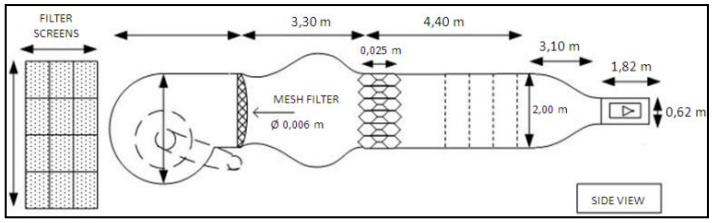

Figure 7. Price-Païdoussis subsonic blow down wind tunnel dimensions.

The maximum flow speed corresponding to Mach number of 0.18 is induced by the engine and the centrifugal double-wheeled fan. Two inlets at the opposite side of the rotor allow entering air by increasing the pressure flow. Using the twenty-four small turbine propellers of the fan, the fan is able to rotate at much higher speeds than regular fans with large blades. The engine and the centrifugal fan are located inside the mechanical room which is soundproof and insulated from debris and dust.

The diffusion section consists of a wide angle diffuser, a large decantation chamber, a contraction section and a tests section. From static pressure buildup, the flow is projected to an oval shaped flow straightener with circular patterns. Then, the flow passes through a series of five filters, where the first filter is honeycomb shaped and the other four filters are square shaped these filters are manufactured in nylon and are positioned at 0.5 m from one another. The decantation section lets a turbulent flow smooth out to a laminar flow. The LARCASE – Price-Païdoussis subsonic blow down wind tunnel has two test sections. The first section is built of wood with two removable Plexiglas doors, and this section, is 0.62 m high, 0.91 m wide and its length is 1.83 m. The maximum Reynolds number is 2.4 million and the maximum Mach number is 0.12. The second test section has the height of 0.31 m, the width of 0.61 m and the length of 1.22 m respectively. Its maximum Reynolds number is 3.5 million and its maximum Mach number is 0.18.

C. Building A Test Wing With a NACA0012 Airfoil

1. Wing Structure Dimensioning Calculations

The wings used during the tests in wind tunnel were built according to a classic design in aeromodelism. For example, a main spar would be able to withstand the maximum load admissible, and was built while the ribs allowed the transmission of applied forces from the surface to the spar, by keeping in mind that those ribs were also defining the airfoil shape. Moreover, a skin covering the airfoil was applied; this skin was manufactured using a protective plastic film (made of MonoKote). The maximum speed used in the large test section of the wind tunnel is 40 m/s. By considering a maximum lift coefficient of 1.5, a safety margin for the NACA0012 airfoil, which maximum lift coefficient is around 1. The air density ρ was set at 1.18 kg/m³ (which was considered as an average value measured in our wind tunnel room), the wing span is 12 in, thus is half of the height of the test chamber and the wing chord is 10 in. By use of the lift force equation for a wing Eq. (1), the maximum lift force of 109.6 N was obtained.

$$L = \frac{1}{2} * \rho * v^2 * C_L * S \tag{1}$$

Bending tests determined the maximum constraint for the balsa wood used. The density of the balsa wood was indicated for each rod by, considering the maximum stress would be proportional to its density. The density was calculated from the weight of the balsa rod and its volume. Thus, by using Eq. (2), the maximum stress sustained by the balsa wood was calculated. In our case, mass at breakage was 21.2 lb and the distance was 24 in. The value of F then became 94.5 N and the value of x was equal to 609.6 mm. The rod used during the test was a stick of rectangular section with a height of 1 in and a width of 0.75 in thus, the inertia moment I_G was equal to 40,647.6 mm4. Finally, the value of y was found to be 12.7 mm.

$$\sigma = \frac{F * x}{I_G} * y \tag{2}$$

The tests defined the maximum constraint σ of 18 MPa (2616 psi) for a density of the balsa wood of 194 kg/m³ (0.007 lb/po³). Using Eq. (3), the needed spar widths could be calculated according to the established thickness of 0.75 in (determined by the chord thickness). The spar height h was 0.75 in, the wing span b was 12 in, the previously calculated lift L was 109.6 N, the maximum constraint σ_M was 18 MPa and the thickness of the upper part of the spar t_u was 0.375 in. Using those informations, the minimum spar width l was calculated, which was to be 0.41 in. According to the standard sizes and available stocks, we chose a spar of 0.75 in high by 1 in wide. Therefore, the necessary information was obtained regarding the required spar for the building of wings accordingly to NACA0012 airfoils.

$$l = \frac{b * L}{h * \sigma_M * t_u} \tag{3}$$

2. Cutting ribs

Firstly, the rib was generated in CATIA V5 using the tool we have designed for this purpose. This tool automatically generates any airfoil in CATIA V5 starting from the airfoil coordinates file. In the sketch thereby generated, the location of the spar section was drawn and the half-circle at the verge as the leading edge rod was too. The diameter of the half-circle was 0.75 in and it was protruded by 0.0625 in on each side of the airfoil accordingly with the surface of the wing which would be added later. The half-circle was positioned as best as possible to follow the airfoil coordinates. Then, the resulting drawing was printed; it was to be the outline for the cutting of the pieces. The necessary thickness of the balsa sheets was 0.0625 in, which was more than enough for the transmission of the forces while having a good sturdiness against ribs handling. A number of sheets corresponding to the number of needed ribs were to be stacked (in this example, six ribs were used along the wing span). A large sheet could be pre-cut in smaller sheets in order to reduce the number of large sheets to be used. For this wing, all the ribs could be cut from a single large sheet of 36 in long by 2 in wide and 0.0625 in thick. The sheet and the pattern from CATIA V5 were attached with masking tape and the set was sawn with an electric cutter (as a Dremel). When laser cutting is possible, it could be used to facilitate the process, and to improve the accuracy of calculations. The generated airfoil by the tool designed by us is constructed of short lines instead of a curve, and allows cutting machines to follow correctly the shape. Using ribs and spar of sections of 0.75 in by 1 in by 12 in long, four large sheets were needed of 0.0625 in thick, 5 in wide and 12 in long and a half-circle rod of 0.75 in of diameter and 12 in long.

3. Bonding pieces for the NACA0012 airfoil

The glue used to bond the balsa pieces is wood glue (Lepage). Thus, between each step of gluing, we had to wait 30 minutes to make sure the previous bondings would stay in place. The first step was to place the ribs along the spar. The intended spacing between the ribs has been calculated with the aim to increase the strength at the root of the wing while optimizing the weight. When the ribs were glued in place, the rod which would serve as leading edge was positioned. If the cuttings were done correctly, the rod protruded of 0.0625 in on each side of the rib. The masking tape maintained the rod in place during gluing. As indicated previously, the masking tape was removed after 30 minutes (therefore, between two operations) in order to perform the operations indicated in the following sections.

The gluing of the surface started from the leading edge. To glue it, the pre-cutted piece of surface should be positioned in order to follow the leading edge. Masking tape and small loads (approximately 1 lb) would make sure the balsa sheet is correctly following the shape of the ribs and is bonding with the entire contact edge. After gluing the first piece of surface, the second part of skin forming the trailing edge is to be placed. In order to achieve a good

finish on the trailing edge, a supplementary thickness of 0.0625 in should stock from the edge of the ribs. After gluing the surface on one side of the wing, the surface on the other side of the wing had to be glued in the same way. When the bonding of the different pieces of the wing is done (ribs, spar, leading edge and surface), junctions between the pieces should be sanded to improve surface finish and to obtain a better airflow around the airfoil. Thus, the trailing edge should be sanded to reduce its thickness. The trailing edge sanding intends to make a chamfer of 0.0625 in on the full-span of the inner and outer surface. The last step in building the airfoil consists in applying the plastic film (MonoKote). This film is a sheet of thermo-retractable plastic. The process is known as it is used in aeromodelism as it protects the balsa.

To be set-up in the wind tunnel, the wing has to be embedded in a disk. Thus, during the application of the MonoKote, a surface margin of half an inch should be kept to glue the wing on the disc (bonding area).

4. Support Discs Manufacturing

A support disc has to be made of wood in order to be glued to the wing. To facilitate its building, the disc could be made of compacted wood which is easier to cut and to sand. In the same way as for the ribs, the plate pattern must be designed with CATIA V5. In order to design it, on the sketch of the airfoil used initially, the chord was increased by 0.125 in (accordingly to the wing surface) and the necessary diameter for setting-up on the current aerodynamic balance interface of 10.7 in was traced for the circle centered around the airfoil.

As a marker to position the wing on the balance, a line should be added corresponding to the angle of attack of 0 °. After cutting the plate, the fitting of the airfoil with the plate should be verified, as well as the adjustment of the plate with the balance. Using the balance plate, four holes must be pierced for the fixation of the wing on the balance, while the zero angle markers must remain correctly positioned.

Once the adjustments on the support plate are done, the airfoil can be glued on it. Once the glue is set, the airfoil is ready to be used in the wind tunnel.

Figure 8. Embedded airfoil on the support disc.

D. Wind Tunnel Test Results

1. Raw Results

After the finalization of the NACA0012 airfoil, it was installed on the aerodynamic balance in order to measure its characteristics. The measurements were made at four different speeds, 20 m/s, 25 m/s 30 m/s and 35 m/s and at angles of attack between -10 ° and 20 °.

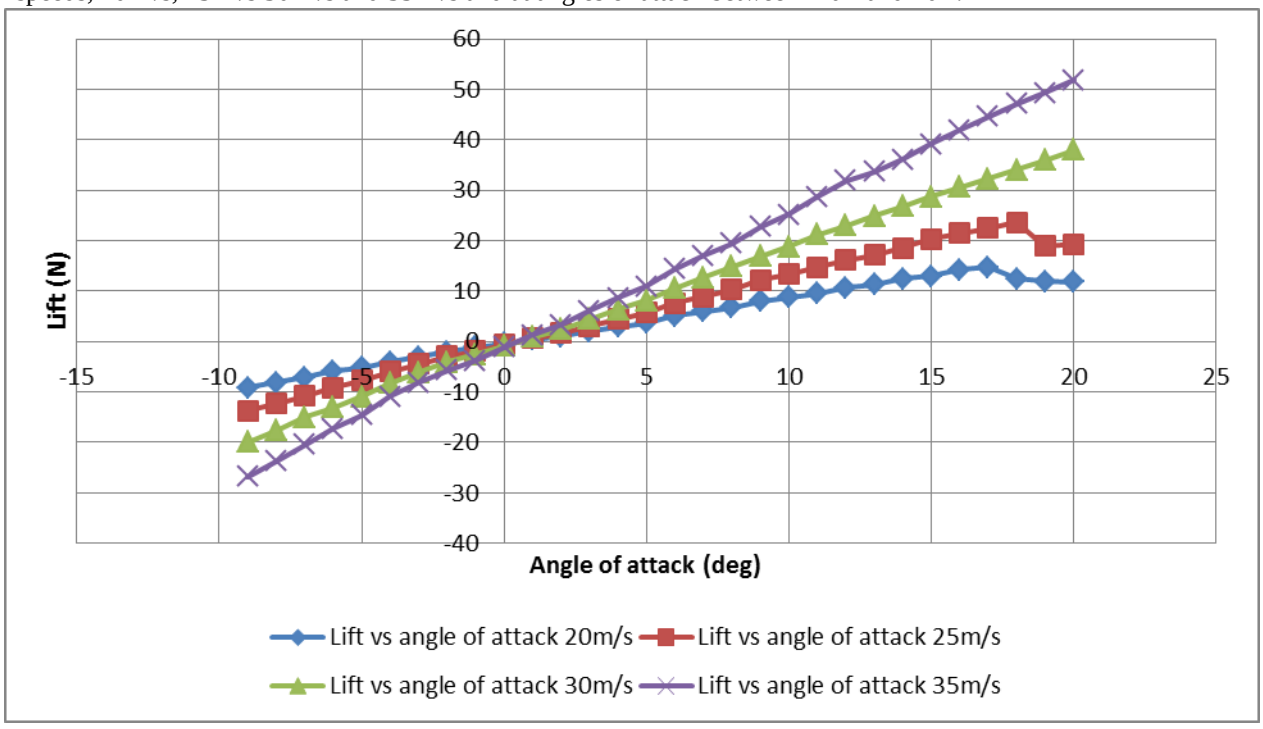

Figure 9. Variation of the lift force with the angle of attack and four speeds between 20 m/s and 35 m/s.

From the measurements performed with the balance, we could directly trace the graphs for the aerodynamic forces variations with the angle of attack α at different tested speeds. Accordingly to the angle of attack and the four speeds between 20 m/s and 35 m/s, figure 9 shows the variation of the lift force, figure 10 shows the variation of the drag force and figure 11 shows the variation of the pitch force.

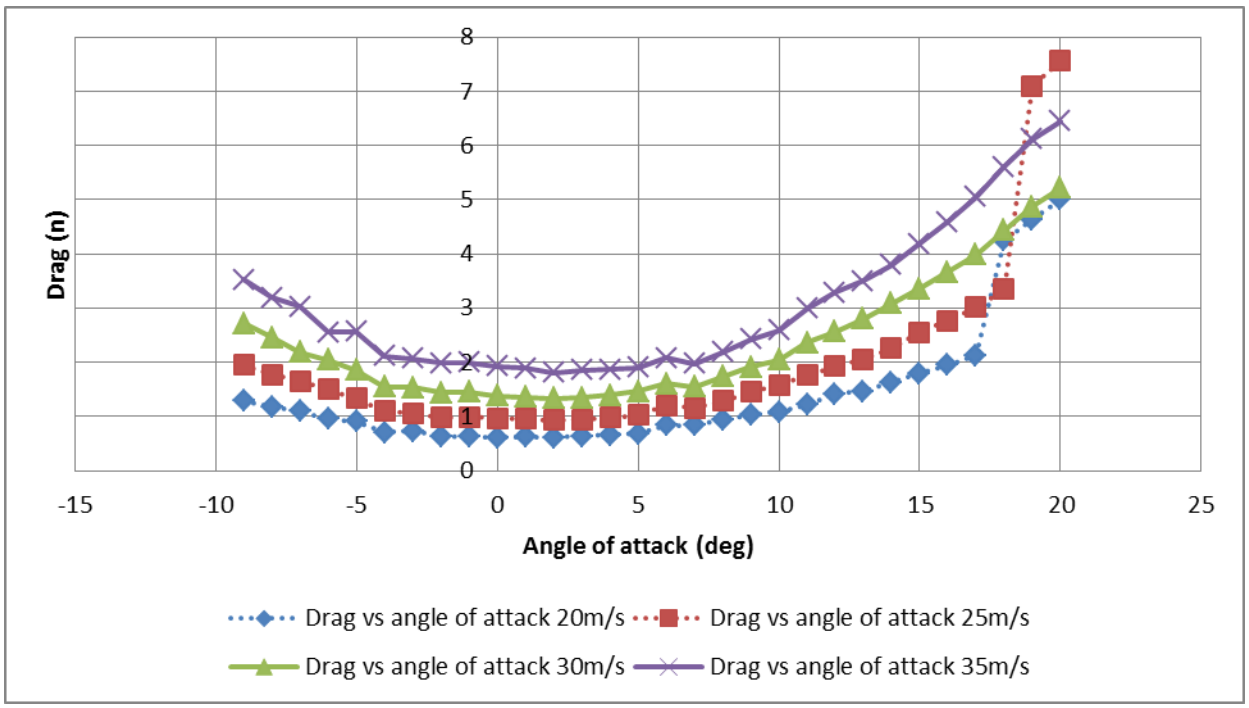

Figure 10. Variation of the drag force with the angle of alpha and four speeds between 20 m/s and 35 m/s.

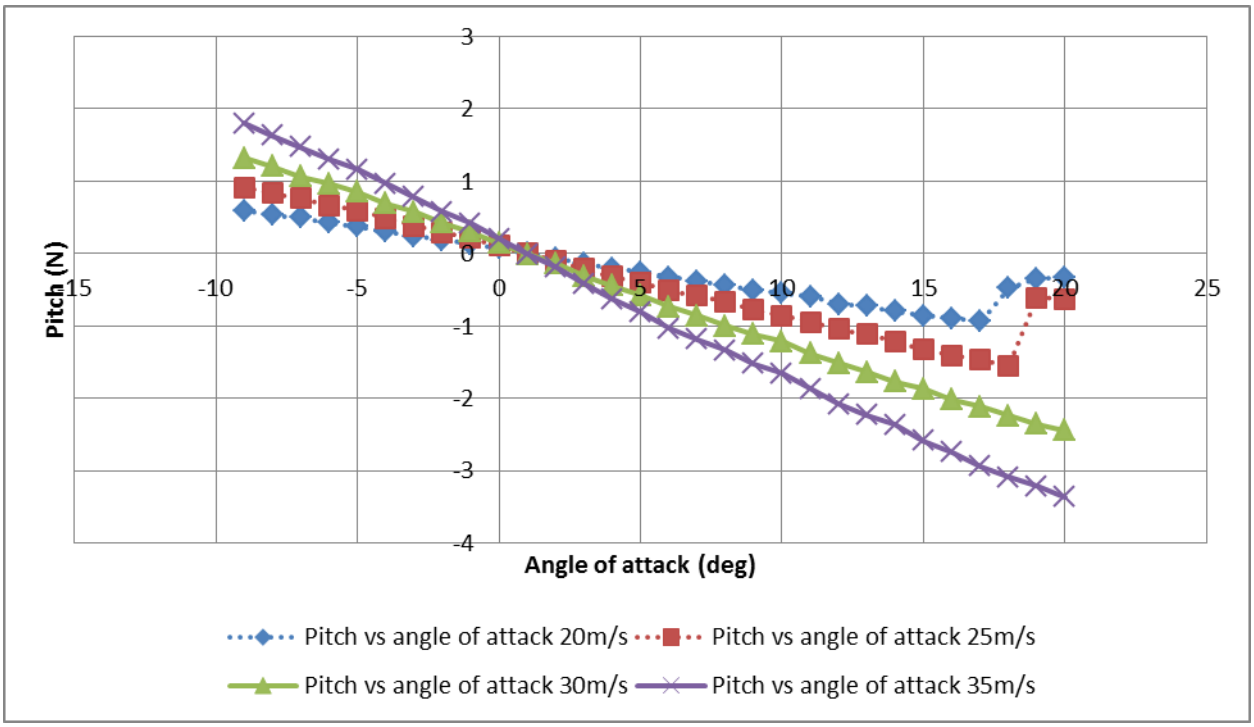

Figure 11. Variation of the pitch force with the angle of attack and for four speed between 20 m/s and 35 m/s.

For the four tested speeds, using Eqs. (4), (5) and (6), the variations with the angle of attack of the tested wing lift, drag and moment coefficients could be calculated.

$$C_L = \frac{2*L}{\rho*v^2*S} \tag{4}$$

$$C_D = \frac{2*D}{\rho*v^2*S} \tag{5}$$

$$C_M = \frac{2*M}{\rho*v^2*S*c} \tag{6}$$

2. Comparison between the experimental results and the theoretical results using the XFLR5 software.

The XFLR5 software was used to obtain the theoretical variation of the lift, drag and moment with angle of attack. The code used by the XFLR5 software to calculate the airfoil performances is the same as XFoil with the only difference being the programming language used.

A calculation based on the airfoil lift, drag and moment variation with angle of attack and on the wing geometry, would allow us to obtain the wing performances quicker than by using a software such as ANSYS-Fluent. Meanwhile, from the analysis of the results, the reliability of the results obtained by the software is estimated and its limits are found.

Following the analysis of differences between theoretical and experimental results, the lift coefficient was found to be correct, the drag coefficient seemed offset and the moment coefficient curves did not have the same slope. In the following sections, we are going to demonstrate the improvement of those results accordingly to physical phenomenons known for the Price-Païdoussis subsonic blow down wind tunnel. An existing stall angle of 18 ° was found at a speed of 20 m/s and of 19 ° at a speed of 25 m/s but we have not noticed any stall angle at the speeds of 30 m/s and 35 m/s during our test.

3. Correction Of Lift Coefficient Of The Wing

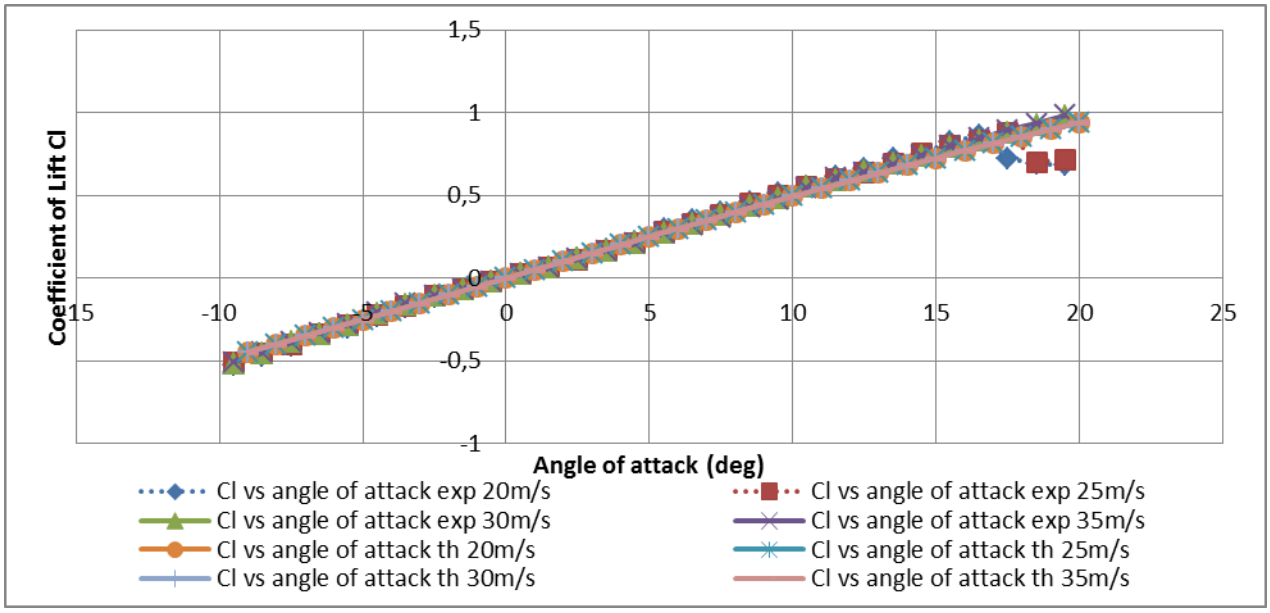

Figure 12. Lift Coefficient Variation With An Applied Correction Of -0,5 ° On The Angle Of Attack alpha.

The positioning of the angle of attack is done manually in the Price-Païdoussis subsonic blow down wind tunnel. Even if the system provides an adequate accuracy to reliably ensure the relative displacement between each measurement, there is still a slight uncertainty related to the starting position. In order to calculate this possible imprecision, the variation of the lift coefficient with the angle of attack was analyzed, especially around the zero angle of attack. Because the NACA0012 airfoil is symmetrical thus, for an angle of attack of 0 °, the lift coefficient should be 0. In our case, the lift coefficient was not equal to 0. Because it was slightly negative, it indicated that the actual angle of attack was also below 0 °. The measured lift force at 1 ° had a similar value to the force measured at 0 °. Therefore, we supposed that the actual 0 ° at midway between 0 ° and 1 °, at 0.5 °. Then an experimental

correction factor of -0.5 ° was applied to the curves of the measured lift, drag and pitching moment forces. Using the -0.5 ° correction, the variation of the lift coefficient with the angle of attack was improved. As shown in figure 12, the corrected curve followed the lift variation corresponding to a symmetrical wing, the lift coefficient and angle of attack were both at 0.

4. Drag Coefficient Correction

An offset around small angles and negative angles and a divergence for wide angles of attacks (off stalling) were measured for the drag coefficient variation. By considering there is no edge effect in the Price-Païdoussis subsonic blow down wind tunnel, the air friction against the plate might have disrupted the drag coefficients values with the angle of attack. Previous experiments on an ATR42 wing showed an existing constant between the theoretical and experimental drag coefficient curves. The constant value was 0.022 for a no-load tray at the speed of 20 m/s. The value was obtained by measuring the drag force while the plate was empty and the speed was at 20 m/s. By considering the upper surface of the balance as the calculation area, it was used in Eq. (5). Then the drag coefficient curve was corrected with the resulting constant. The corrected experimental curves were closer to the theoretical ones, especially for the drag coefficient with angle of attack at 20 m/s, the speed at which the coefficient has been calculated. The correction of the divergence around high angles for speeds greater than 20 m/s was to be determined.

The divergence between the curves increased with speed but also with the angle of attack. The divergence according to the angle of attack could be explained by the exposure of the plate surface to the airflow. A part of the plate was not directly in the airflow as the angle of attack was increased. The relationship between the angle of attack and the divergence was established by tracing the curve of the deviation between the drag coefficients for the speeds of 25 m/s, 30 m/s and 35 m/s against 20 m/s, at each angle of attack. The curve showed a consistent symmetrical tendency of the divergence according to the symmetrical property of the wing. This tendency could not be kept for angles greater than 16 ° because of the wing stall at 16 °. Only angles between 0 ° and 16 ° were used to establish the analytical curve of variation. By visualizing the variation curves of the drag coefficient with the angle of attack, the obtained straight lines described a linear relationship for those variations. The linearization slopes increased steadily of approximately 0.0006 from one curve to the other. To establish a constant relationship between the speed and the variation of the drag coefficient, the gap between the curves of 20 m/s and 25 m/s should have been the same as between 25 m/s and 30 m/s, and as between 30 m/s and 35 m/s. The slopes were close with a mean value at 0.0006 which was the difference between 30 m/s and 35 m/s. The curve between 30 m/s and 35 m/s was steadier than the others and it did not stall until 20 ° and thus, it was used to define the linear correction according to the angles of attack and speeds. A relationship was established between the gap of the drag coefficient against speed build-ups of 5m/s starting at 20 m/s. There were few information concerning the negative angles. Since the variation was considered symmetrical, the slope of the curve should have been the same as for the positive angles. The positive angles equation for a variation of 1 m/s was obtained by dividing the previous linear equation by 5:

$$y = \frac{-0.0006x + 0.0015}{5} = -0.00012x + 0.0003 \tag{7}$$

The correction relationship became as follow :

$$\begin{cases} If\ v \leq 20\,m/s \rightarrow correction = 0.022 \\ If\ v > 20\,m/s \rightarrow correction = (-0.00012 * abs(\propto) + 0.0003) * (v - 20) + 0.022 \end{cases} \tag{8}$$

As shown in figure 13, this correction adjusted the divergence related to speed. The experimental curves of drag coefficients matched with the theoretical curves. More tests with other airfoils were done to validate the consistency of the deviation.

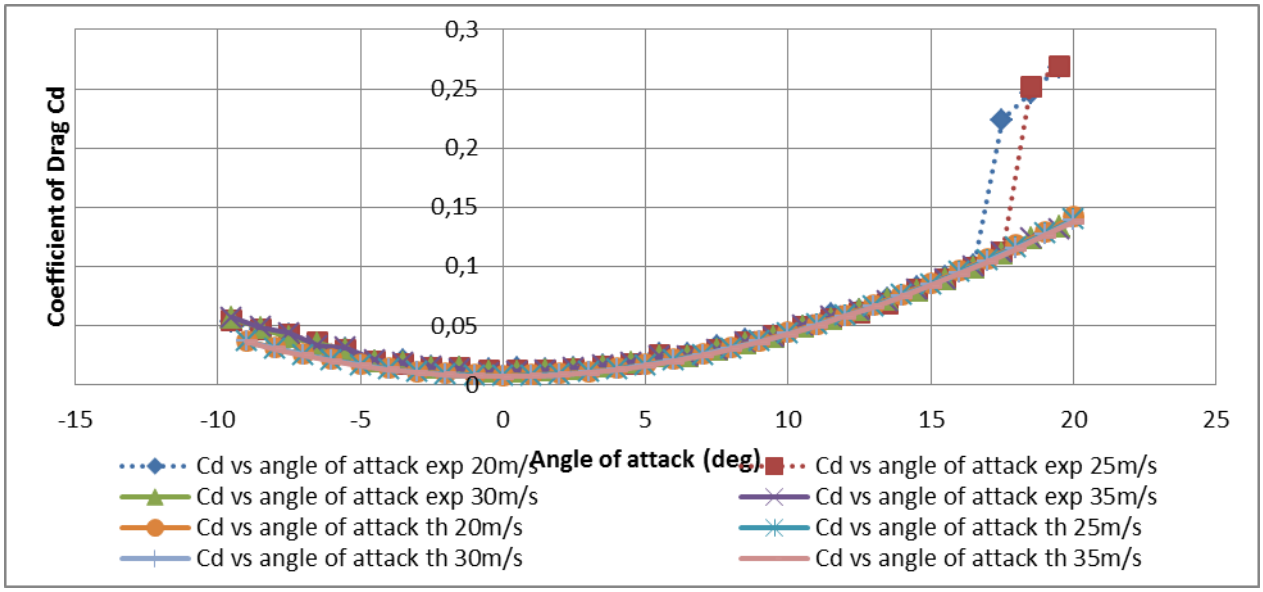

Figure 13. Corrected Variation of drag coefficient with angle of attack.

5. Correction Of The Airfoil Moment Coefficient

As shown in figure 13, this correction adjusted the divergence related to speed. The experimental curves of drag coefficients matched with the theoretical curves. More tests with other airfoils were done to validate the consistency of the deviation. The experimental variation of the moment coefficient with the angle of attack was linear but the slope was different from the theoretical curve. The theoretical moment coefficients were given at a position of ¼ of the chord. In the wind tunnel, the moment coefficients were measured at ½ of the chord. To correct that disparity, we used Eq. (9). By applying the equation to the experimental curve of the moment coefficient at 50% of the chord, we got the experimental moment coefficient at 25% of the chord.

$$C_{M_{1/4}} = C_{M_{1/2}} + \frac{corde}{4} * C_l \tag{9}$$

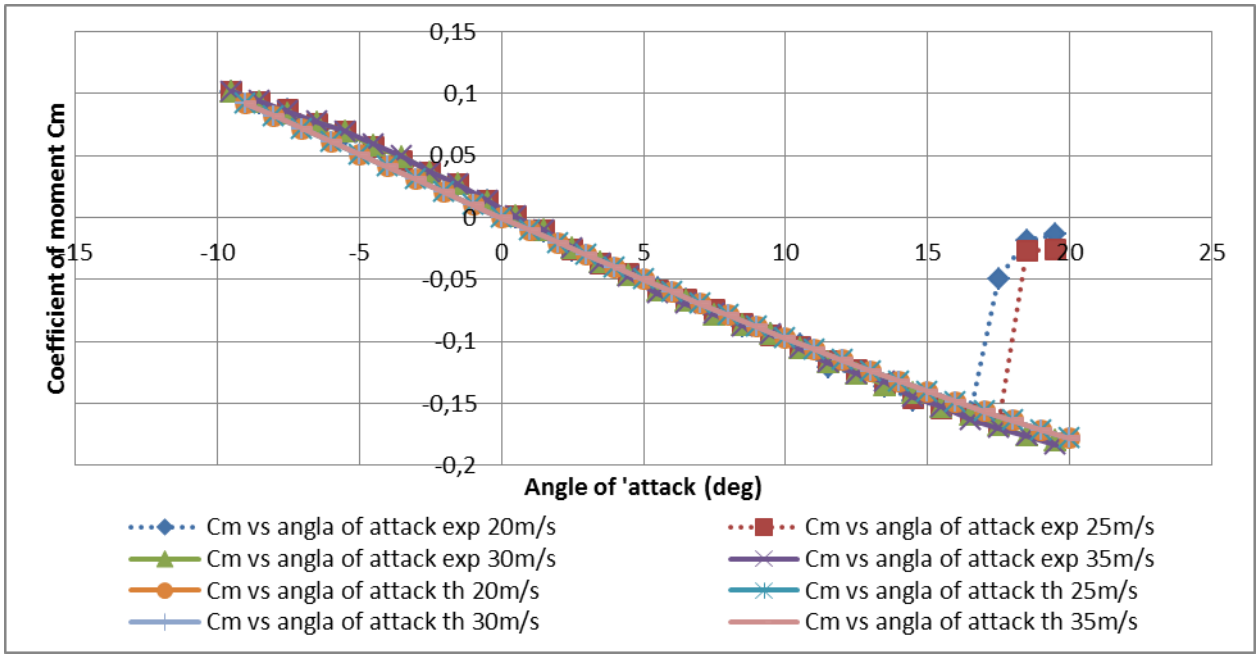

Figure 14. Moment Coefficient vs the angle of attack alpha at 25% of the chord.

In figure 14, the adjusted curves for the measured moment coefficient showed that the experimental moment coefficient was corrected accordingly to the theoretical moment coefficient.

IV. Creation And Analysis On CATIA V5

By using the CATIA V5 software, the structural analysis of the studied wing could be performed. In order to automate the methodology, as to simplify the manipulations in the software and as to substantially gain in time, tools have been created as part of this project. The analysis suggested in this paper focuses on the study of the constraints acting on the wing. By Eq. (2), the stresses depend on the wing shape and on the applied forces but not on the material used. Then the wing can be studied without any knowledge of (or by ignoring) the exact properties of its constituents materials. This premise greatly simplifies the wing analysis, allowing the wing to be modelized as a single and complete part, as opposed to an assembly. Subsequently, each material used for each part of the wing was checked against the associated localized constraints. The next section describes the methodology and the equations used by the created tool.

A. Generation of the surface on CATIA V5

The tool designed on CATIA V5 creates in three steps the surface for the wing dimensioning. Firstly, the value tables in the text file exported from XFLR5 are imported in CATIA V5. From those values, the airfoils coordinates at the wing root and tip are extrapolated and the wing span is determined. Then sketches of the airfoils are created at the wing root and tip and another sketch is created as a guide curve for the surface grid. The guide curve is essential to the creation of the wing, it links the trailing edge point at the root of the wing and the corresponding trailing edge point at the tip of the wing. Lastly, the volume is created from the three previous sketches and a wing shell is created as an outer surface. Once the wing surface is created, the pressure coefficients are determined on each cell of the surface of the wing accordingly to the distribution given by the XFLR5 analysis. Because of the large number of applied coefficients, the computing process is automated instead of manually calculated. Then, a fixture is applied on the surface corresponding to the wing root. Once the internal structure of the wing will be created, the position of the fixture will be modifiable to fit how the wing shall be embedded with the fuselage of the aircraft. With this model, the created surface with its pressure coefficients has the advantage of being parametrically modifiable. Each point of the wing chord or of the wing span could be individually modified. Air speed and air density can also be modified.

1. Automatic Generation of The Wing Airfoil

In order to create the wing surface, the airfoil coordinates are determined for the wing to be created. The coordinates must fit the meshes of the grid and thus; we cannot use the coordinates of the initial airfoil. The airfoil shape has been extrapolated from the coordinates of the pressure points distributed around the wing. Firstly, the mesh used by XFLR5 was considered uniform throughout the chord and the span. By knowing that each application point of pressure is at the center of a corresponding mesh and that the trailing edge point is at coordinate (1,0), all other coordinates of the airfoil can be determined. The extrapolation of the chord coordinates depends on the dihedral angles and depends on wing sweeps. The airfoil coordinates for the wing root and tip were obtained as described. For each coordinate, the X (width) and Y (height) components were calculated. Here are the equations used for the calculation:

$$X_{tip,i} = Offset + Nbr1_i * C_{tip} \tag{9}$$

$$Y_{tip,i} = \tan(dihedral) * Span + Nbr2_i * C_{tip} \tag{10}$$

$$X_{root,i} = Nbr1_i * C_{root} \tag{11}$$

$$Y_{root,i} = Nbr2_i * C_{root} \tag{12}$$

Where :

$$Nbr1_i = \frac{2 * (CP_{Xroot,i} - a1 * CP_{Yroot,i})}{C_{root}} - Nbr1_{i-1}$$

$$Nbr2_i = \frac{2 * (CP_{Zroot,i} - a2 * CP_{Yroot,i})}{C_{root}} - Nbr2_{i-1}$$

$$a1 = \frac{CP_{Xtip,i} - CP_{Xroot,i}}{CP_{Ytip,i} - CP_{Yroot,i}}$$

$$a2 = \frac{CP_{Ztip,i} - CP_{Zroot,i}}{CP_{Ytip,i} - CP_{Yroot,i}}$$

$$Nbr1_{init} = 1 \; et \; Nbr2_{init} = 0$$

$$Nbr1_{final} = 1 \; et \; Nbr2_{final} = 0$$

The airfoil coordinates for the wing root and tip are obtained with those equations. The corresponding sketches of the root and tip airfoils are created with those coordinates. When the wing is created, the airfoil is modifiable hence optimizable since coordinate parameters were created for each point of the airfoil. The coordinates are dimensionless. With the aim to enable modifications to the wing chord, an additional parameter corresponding to

each airfoil chord was created. Then without importing again new coordinates and without starting over the wing design modifications could be done. In order for the parametrization to work correctly, each point in the sketch must be constraint according to its calculated X and Y coordinates and relations with geometric parameters of the wing are created.

$$Y_i = \frac{Nbr1_i * Span}{FactorD * \cos(dihedral)} \tag{13}$$

$$X_i = C_{root} - \frac{Y_i * \cos(dihedral) * \left(C_{root} - \left(C_{tip} - Offset\right)\right)}{Span} + guide\_offset \tag{14}$$

Where :

$$Nbr1_i = -2 * CP_{Y(root-i+2),0}$$

$$FactorD = Nbr1_{final}$$

$$guide\_offset = \begin{Bmatrix} 0.00001\ si\ i\ paire \\ 0\ si\ i\ impaire \\ 0\ si\ i\ final \end{Bmatrix}$$

An extrapolation from the wing pressure coefficient coordinates is performed in order to get the wing span, the dihedral angle and the wing offset (offset of the leading edge at wing tip). The equations used are as follow:

$$C_{root} = \frac{pos\ C_{root} * -CP_{Y,tip} + CP_{Y,root} * pos\ C_{tip}}{-CP_{Y,tip} + CP_{Y,root}} \tag{15}$$

$$alpha = \tan^{-1}\left(\frac{CP_{Xtip,0} - CP_{Xroot,0}}{-CP_{Y,tip} + CP_{Y,root}}\right) \tag{15}$$

$$Span = \frac{\left(-CP_{Y,tip} - CP_{Y,root}\right)}{\cos(alpha)} \tag{16}$$

$$C_{tip} = \frac{pos\ C_{root} * \left(-CP_{Y,tip} - CP_{Y,root}\right) - C_{root} * -CP_{Y,tip}}{-CP_{Y,root}} \tag{17}$$

$$Offset = \frac{CP_{Xtip,0} - CP_{Xroot,0}}{0.00254} \tag{18}$$

$$Dihedral = \tan^{-1}\left(\frac{CP_{Ztip,0} - CP_{Zroot,0}}{-CP_{Y,tip} + CP_{Y,root}}\right) \tag{191}$$

From those equations, coordinates were obtained for the curve that serves as guide for the wing volume. During the creation of the sketch, each point is restrained by two conception constraints bound to the coordinates, and those constraints are linked to the geometric parameters of the coordinates by a formula. Those formulas bind the guide curve to follow any modification made to the wing dimensions.

2. Generation of the final surface

The generation of the wing surface is finalized by the construction of the wing volume and the shell, creating the final surface. The volume was constructed with the creation tool for solids by multi-sections. The previous sketches for the airfoils and for the guide were used with the creation tool. Those operations created a volume corresponding to the outer dimensions of the wing. The outer surface of the volume is decomposed into a grid concordant with the initial XFLR5 grid. Then, a shell, casting the volume, was applied. This shell is the final surface obtained as the outer skin of the wing. The default thickness was 0,0625 in but could be changed accordingly to the optimization of the wing structure. For the wing analysis, the default material applied is aluminum. By knowing that the analysis of constraints does not change significantly with the material used, it is not necessary to change the material for the studied wing.

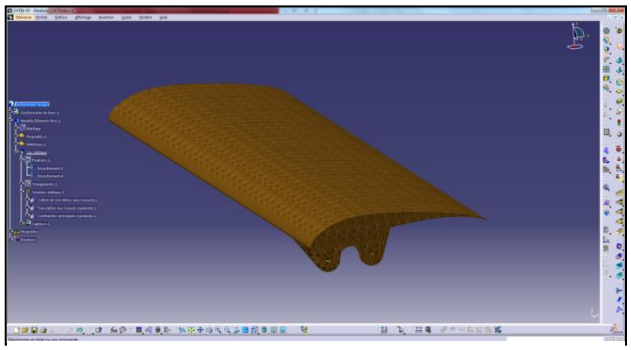

Figure 15. Test Half-wing.

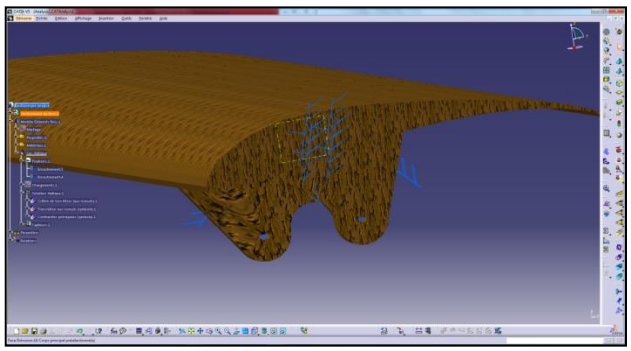

Figure 16. Fixation of the wing by the spar and by fastening holes.

3. Application of pressure coefficients on the wing surface

The last important step of the automation program is to automatically apply pressures around the surface of the wing. Each mesh of the grid on the wing surface was assigned its corresponding pressure. In the CATIA V5 model, every surface of the wing can be retrieved by its Boundary Representation (B-Rep) and each pressure is saved in a pressure parameter. Those parameters depend on the speed and density of the air and depend on the associated pressure coefficient. By using those parameters it is possible to vary the pressure applied on the wing accordingly with the speed and density of the air. The B-Rep of each surface of the wing must be known for the modifications to work. The automation of the generation of the wing surface was necessary, if done randomly during the fabrication process, the B-Rep values would have been different and thus, it would not have been possible to automatically assign the pressure values. Then the distribution of the pressures was applied automatically on the wing and it could be modified accordingly with the dynamic air pressure parameters.

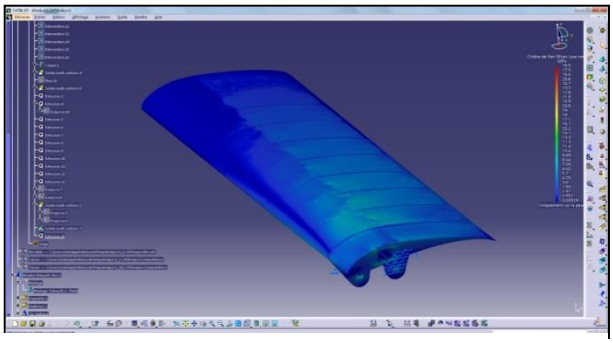

Figure 17. Display of Von Mises Constraints.

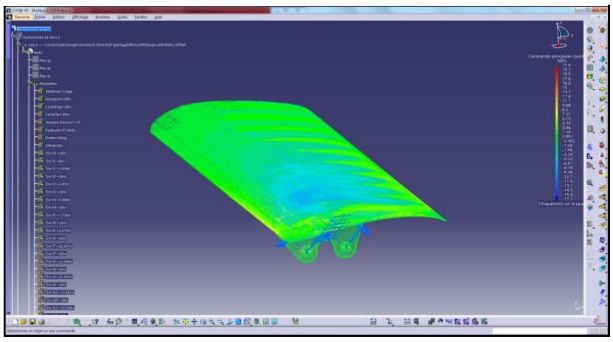

Figure 18. Display of the main constraints – Traction (red), Compression (blue).

B. Creation of the wing structure

Once the surface is generated with its applied forces, the wing structure inside of that surface can be created. Since the structure is comprised of ribs with a main spar, the surface workbench could be used to construct the ribs and the volume workbench could be used to construct the spar. Accordingly to the designed wing thickness, it is possible to vary the thickness of the wing shell. In the example of figure 15, ten ribs were added and distributed evenly and a hollow spar of rectangular section was positioned at ¼ of the chord. Then, a supplementary thickness of 0.0625 in was added at the leading and trailing edges as to fit structural reinforcements and the second rib was prolonged as to attach the wing to the fuselage. The fixtures were modified as to better correspond to the actual specifics of the final assembly (figure 16). The default fixture was removed, then another fixture was positioned at the spar as to stand for the continuity of the spar on the second half of the wing and also, two more fixtures were added corresponding to screws meant to attach the wing on the fuselage from the second rib.

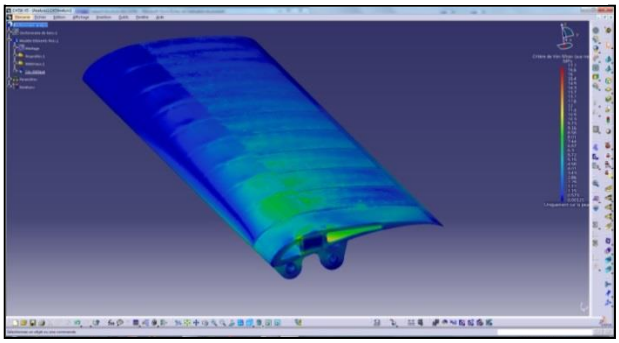

Figure 19. Von Mises Stressses after optimization.

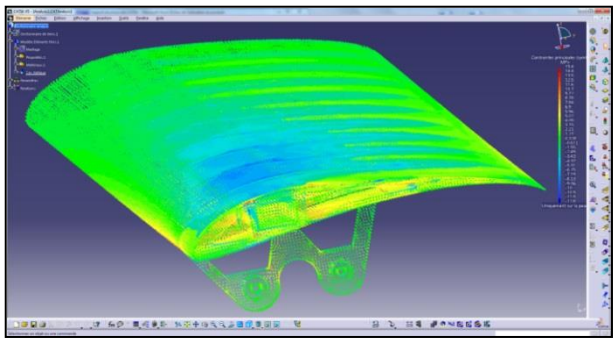

Figure 20. Main Contraints after optimization.

C. Result Analysis

The finite-element analysis in CATIA V5 was used to study the stresses sustained by the material and the displacements of the material. By using a parabolic mesh, the buckling in the material could be identified, this being a necessary information to the structural analysis of a wing. As to facilitate the analysis, the wing was designed in a single material which considerably sped up the computation time. Furthermore, as long as the analysis remained within the elastic range of the material, the applied constraint could be considered not dependent on the material used. There is two methods used to visualize the constraints, by the Von Mises criterion (figure 17) and by

the main constraints values (figure 18). With the main constraints, the compression and tension areas were identified as to determine if the structure would well resist to both constraints. However, the operation required more computational resources to display the results than the Von Mises criterion method. This last method provides a better visual rendering and can be used to identify more easily the areas of stress concentrations in the structure.

D. Structure Optimization

The first analysis identifies the structure characteristics, the areas sustaining significant stresses as well as the areas undergoing only little constraint. With those information, the structure could be optimized. For example, the ribs were hollowed but their thickness was increased for those close to the root. The spar size at the root was increased and it was reduced at the wing tip. There are two approaches for optimizing the structure, by applying the maximum load and a security factor on the maximum stress, or by applying the security factor on the load and then adjust the maximum stresses at the limits of the material. The objective was to reduce the thickness of the structural components to reduce the weight of the structure while maintaining sufficient strength. After optimization, the amplitude of stresses had decreased, and the stress distribution was more uniform. There should be less stress concentrations.

E. Comparison between real resulting forces and the forces in CATIA V5

With the structural calculation in CATIA V5, it is possible to generate a final report giving information about the number of nodes in the mesh, the quality of the mesh elements, the properties of the materials used, a summary of the calculations and the forces and moments applied on the wing. To compare the applied forces on the model against the real forces, we used the tables of forces provided in the CATIA report. The Table 3.1 shows the forces for the CATIA model of the NACA0012 tested in wind tunnel at the angle of 15 ° and a speed of 20 m/s. In the wind tunnel, the measured lift force was 12.9 N, and the CATIA analysis was giving a force of 12.83 N, meaning a 0.5% error. However, the measured drag force was 1.42 N after correction, and in CATIA the force was 1.7 N, thus an error of 19.7%. If we consider the YZ plan, the force in CATIA was $\sqrt{12.833^2 + 1.7011^2} = 12.94\ N$ and the measured force was $\sqrt{12.9^2 + 1.42^2} = 12.98\ N$. The error on the forces applied on the structure was 1.1%. That validates the model developed in this paper.

Table 1. Applied forces on the CATIA model.

Composantes	Forces Appliquées	Réactions	Résidus	Erreur Relative
Fx (N)	-6.2312e-004	6.2312e-004	-1.4939e-011	7.5089e-012
Fy (N)	-1.7011e+000	1.7011e+000	5.5105e-012	2.7698e-012
Fz (N)	1.2833e+001	-1.2833e+001	2.6911e-010	1.3526e-010
Mx (Nxm)	6.3010e-001	-6.3010e-001	2.1213e-011	3.6507e-011
My (Nxm)	1.6019e+000	-1.6019e+000	6.1764e-011	1.0629e-010
Mz (Nxm)	2.0662e-001	-2.0662e-001	-3.0864e-012	5.3117e-012

F. Modification of parameters in the model

With the model generated in CATIA, there was liberty concerning the dimensions of the wing and the aerodynamic characteristics such as air speed or air density. That way we adjusted the wing chord at the root or at the tip, its span, the dihedral angle in the wing or the sweep angle. This parametrization enabled slight modifications of the wing without having to redo the structure and the analysis in whole. With the parametrization of the speed, we could adjust the force sustained by the model and test the strength of the structure at different load factors.

V. Conclusion

In this paper, we have described our new methodology for a high precision calculation and an application of aerodynamic forces on a wing. As we have seen during the validation of the model, we obtained a precision of 1.1%

on applied forces in the model against forces measured in wind tunnel. It can be concluded that with the suggested methodology it is possible to analyze the distribution of the forces sustained by the wing structure accurately. With the tools that were developed in the scope of this methodology, we can perform analysis really quickly. With this methodology (aerodynamic analysis on XFLR5 and structural analysis on CATIA V5), we can do the conception and the analysis of a wing within half a day while it took many weeks with the previous method (aerodynamic analysis on ANSYS-Fluent and structural analysis on HyperMesh). Another advantage of this methodology is the flexibility of the model used. With the parametrization of geometric dimensions and airflow characteristics in the structural analysis, we gain more freedom during the design of the wing. We can start an analysis of the internal structure of the wing even if we are not sure of its final geometric dimensions or its extreme flight conditions. With our new methodology, we have fulfilled three objectives: an increased accuracy for a structural analysis of a wing, a reduction of the duration of the analysis and a better flexibility of the model. Those improvements allow us to say that this new methodology is a good alternative to the old methods for performing structural analysis of a wing.

Acknowledgements

We would like to thank the Natural Science and Engineering Research Canada (NSERC) for the funds received in the Canada Research Chair for Aircraft Modeling and Simulation Technologies.

References

[1] Bernhammer, L.O., Teeuwen, S.P.W., De Breuker, R., van der Veen, G.J. et van Solingen, E. 2014. « Gust load alleviation of an unmanned aerial vehicle wing using variable camber ». In *Journal of Intelligent Material Systems and Structures*, vol. 25, n 7, p. 795-805.

[2] Li, J., Yang, W., Zhang, Y., Pei, Y., Ren, Y., Wang, W., 2013. « Aircraft vulnerability modeling and computation methods based on product structure and CATIA ». *Chinese Journal of Aeronautics*, vol. 26, n 2, p. 334-342.

[3] Mosbah, B. A., Flores Salinas, M., Botez, R., Dao, T.-M., 2013. « New Methodology for Wind Tunnel Calibration Using Neural Networks - EGD Approach ». *SAE International Journal of Aerospace*, vol. 6, n 2.

[4] Silisteanu, P. D., Botez, R. M. 2010. « Transition-flow-occurrence estimation : A new method ». *Journal of Aircraft*, vol. 47, n 2, p. 703-707.

[5] Rajagopal, S, Ganguli, R. 2011. « Computer Modeling in Engineering & Sciences ». vol. 81, n 1, p. 1-34.

[6] Ben Mosbah, Abdallah, Botez, Ruxandra M., Dao, T.M. 2013. « New methodology for calculating flight parameters with neural network – EGD method ». *AIAA Modeling and Simulation technologies (MST) Conference*. p. 9.

[7] Popov, A. V., Botez, R.M., Mamou, M., Mebarki, Y., Jahrhaus, B., Khalid. M., Grigorie, T.L., 2009, *Drag reduction by improving laminar flows past morphing configurations,* AVT-168 NATO Symposium on the Morphing Vehicles, Evora, Portugal, 20-23 April.

[8] Botez, R. M., Molaret, P., Laurendeau, E., 2007, *Laminar Flow Control on a Research Wing Project Presentation Covering a Three Year Period,* CASI Aircraft Design and Development Symposium, Toronto, Ontario, Canada, 25-26 April.

[9] Grigorie, L. T., Popov, A. V., Botez, R. M., Mamou, M., Mébarki, Y., 2011, *Smart concepts for actuation system and its control in a morphing wing,* 13th National Conference Caius Iacob in Fluid Mechanics and Technological Applications, INCAS, Bucharest, Roumanie, 29-30 September.

[10] Sainmont, C., Paraschivoiu, I., Coutu D., Brailovski, V., Laurendeau, E., Mamou, M., Mebarki, Y., Khalid, M., 2009, *Boundary Layer Behaviour on a Morphing Airfoil: Simulation and Wind Tunnel Tests*, CASI AERO'09 Conference Aerodynamics Symposium.

[11] Grigorie, L. T., Botez, R. M., Popov, A.V., 2012, *Design and experimental validation of a control system for a morphing wing,* AIAA Atmospheric Flight Mechanics conference, Invited session paper, Minneapolis, MI, USA, 13-17 August.
[12] Grigorie, L.T., Botez, R. M., Popov, A.V., Mamou, M., Mébarki, Y., 2011, *A new morphing mechanism for a wing using smart actuators controlled by a self-tuning fuzzy logic controller*, AIAA Centennial of Naval Aviation Forum: 100 Years of Achievement and Progress, Virginia Beach, VA, USA, 20-22 September.

[13] Popov, A.V., Botez, R.M., Grigorie, T. L., Mamou, M., Mebarki, Y., 2010, *Real time airfoil optimization of a morphing wing in wind tunnel,* AIAA Journal of Aircraft, Vol. 47(4), pp. 1346-1354.

[14] Popov, A.V., Botez, R. M., Grigorie, T. L., Mamou, M., Mebarki, Y., 2010, *Closed loop control of a morphing wing in wind tunnel*, AIAA Journal of Aircraft , Vol. 47(4), pp. 1309-1317.

[15] Michaud, F., Joncas, S., Botez, R. M., 2013, *Design, Manufacturing and Testing of a Small-Scale Composite Morphing Wing,* 19th International Conference on Composite Materials, Montréal, Québec, Canada, July 28 – August 2

[16] Silisteanu, P. D., Botez, R. M. (2010). *Transition-Flow-Occurrence Estimation: A New Method. Journal of Aircraft, 47*(2), 703-708.

[17] Popov, A.V., Botez, R.M., Labib, M., 2008, *Transition point detection from the surface pressure distribution for controller design*, Journal of Aircraft, vol.45, no.1, January - February 2008.